

Pion-Nucleon Scattering and the π NN Coupling Constant in the Chiral Color Dielectric Model

Dinghui Lu, Shashikant C. Phatak* and Rubin H. Landau

Department of Physics, Oregon State University, Corvallis OR 97331, USA

(September 19, 2018)

Abstract

We apply the chiral color dielectric model to low- and medium-energy scattering within the coupled π N and $\pi\Delta$ system. Dynamic baryon states in which quarks are confined by the scalar color-dielectric field are constructed in Fock space. Spurious motion of the center of mass is eliminated by constructing momentum eigenstates via a Peierls-Yoccoz projection. The relativistic Lippmann-Schwinger equation is solved for the complex energies of the T matrix poles, and the pole positions of the nucleon and delta are used to fix the few parameters of the model. The S - and P -wave phase shifts, the bare N and Δ masses, the renormalized π NN and π N Δ coupling constants, and the π NN and π N Δ vertex functions are predicted.

* Permanent address: Institute of Physics, Sachivalaya Marg, Bhubaneswar INDIA

I. INTRODUCTION

From their first introduction, quark models have been extensively used to study baryon spectra. Some models have the quarks bound by a potential [1], others have them confined to a bag [2], and others have them bound as solitons [3]. These models are fairly successful at fitting the masses and static properties of the baryon octet and decuplet and even some higher excited states. In most quark models, the baryon masses are identified with the bound state energies of quarks within some potential well. This means that the pion-baryon interactions do not directly affect the values of the baryon masses, and that the baryons are stable since decay channels are not coupled in. Phenomenologically, the masses of excited baryons are determined as the resonance energies in the phase-shift analysis of pion-nucleon scattering. These experimental masses naturally include mass shifts due to the pion-baryon interactions as well as widths due to the finite lifetimes of the states. Accordingly, there are uncertainties in a direct comparison of the experimental masses to the bound-state energies of quarks bound in a potential well.

Chiral models, such as the cloudy bag models [4], contain pions in additions to quarks, and therefore also contain elementary pion-quark interactions. The calculation of masses with these models consequently include shifts due to the pion-baryon interactions. However, these models usually use perturbation theory to calculate the widths of the excited baryons, and this means that higher-order terms are ignored and that unitarity in the pion-nucleon channel is not ensured. Ideally, one should determine the masses and widths of excited baryons by calculating the pion-baryon scattering matrix for a given model, and then finding the complex energies at which the scattering matrix has poles. This approach was used by Thomas, Théberge and Miller [5] for the N - Δ system, and later extended to other partial waves [6] and to other mesons [7].

Bag models suffer from several limitations. First, the use of an artificial bag to confine quarks leads to wave functions which have sharp discontinuities at the bag boundary. This leads to pion-baryon form factors (and ultimately potentials) which have unphysical oscil-

lations and, presumably, limited ability to describe the scattering data. In addition, bag calculations treat the bare baryon masses and the bag radius as independent parameters even though we know this is not correct since for massless quarks the baryon masses are inversely proportional to the bag radius [2].

In the present work the chiral color dielectric model (CDM) is employed to overcome some of the limitations of bag models. The CDM was first introduced phenomenologically to simulate the absolute confinement of quantum chromodynamics (QCD). A connection with the more fundamental theory was established by Nielson and Patkos [8] who found that an effective color dielectric field does indeed arise naturally in lattice QCD after defining “coarse grained” effective field variables. The color dielectric field takes into account the long distance behavior of the QCD vacuum and produces a natural confinement of the quarks within baryons. More recently, Krein et al. [9] have solved the Schwinger-Dyson equation and shown how confinement and a pseudoscalar meson (Goldstone boson) arise if chiral symmetry is dynamically broken.

In some recent CDM models, chiral symmetry is restored via a nonlinear realization which introduces an elementary pion field as a Goldstone boson. Even though the mesons in these models are elementary, the baryon structure and the resulting relations of coupling constants are determined by the quark model [10,11]. In application, the CDM is similar to the cloudy bag model [4,11], yet somewhat more microscopic in its dynamic mechanism for quark confinement and its treatment of baryon recoil within a nontopological-soliton solution to the field equations. Accordingly, when in the present paper we compare models which differ mainly in their treatment of quark binding, we hope to determine how important are improved (or maybe just different) quark dynamics when calculating two-body scattering, and how might the differences in the models manifest themselves.

Our calculation proceeds as follows. First we solve the quark and dielectric field equations of CDM in the mean field approximation (MFA). We then quantize the classical dielectric field using the coherent state, and improve upon the MFA by including one-gluon exchange corrections perturbatively. We include the recoil of the baryon via the prescription of Peierls-

Yoccoz projection [12]. This, presumably, is a more important correction to scattering where large momentum transfers can occur than for static properties where the momentum transfers are small. Once we have bare baryons constructed from quarks within a binding field, we expand the quark-pion interaction in powers of the pion field and calculate the transition matrix elements for baryon coupling with multiple pions. From these we identify the pion-nucleon potential, and then dress the vertices by substituting the potentials into the relativistic Lippmann-Schwinger equation [7]:

$$T_{\beta\alpha}^{LJI}(k', k) = V_{\beta\alpha}^{LJI}(k', k) + \frac{2}{\pi} \sum_{\gamma} \int_0^{\infty} dp \frac{p^2 V_{\beta\gamma}^{LJI}(k', p) T_{\gamma\alpha}^{LJI}(p, k)}{E + i\epsilon - E_{\gamma}(k)}. \quad (1)$$

Here the superscripts LJI indicate the orbital angular momenta, the total angular momenta, and the total isospin, and the subscripts β and α indicate the πN or $\pi\Delta$ channels. We adjust the parameters of color dielectric model so that the poles of T matrix elements occur at the nucleon mass and at the Δ 's complex mass. We then use the model to predict low- and medium-energy πN scattering in S and P waves and the πNN and the $\pi N\Delta$ coupling constants.

II. CHIRAL COLOR DIELECTRIC MODEL

The CDM Lagrangian we choose to use is: [10]

$$\begin{aligned} \mathcal{L} = & \bar{q} \left[i\gamma^{\mu} \partial_{\mu} - \frac{m_q}{\chi} e^{i\gamma_5 \vec{\tau} \cdot \vec{\phi}/f} - \frac{g}{2} \lambda_a \gamma^{\mu} A_{\mu}^a \right] q \\ & - \frac{\kappa(\chi)}{4} (F_{\mu\nu}^a)^2 + \frac{\sigma_v^2}{2} (\partial_{\mu} \chi)^2 - U(\chi) \\ & + \frac{(D_{\mu} \vec{\phi})^2}{2} - \frac{m_{\pi}^2 \vec{\phi}^2}{2}, \end{aligned} \quad (2)$$

$$\kappa(\chi) = \chi^4, \quad (3)$$

$$D_{\mu} \vec{\phi} = \hat{\phi} \partial_{\mu} \phi + f \sin \frac{\phi}{f} \partial_{\mu} \hat{\phi}, \quad (4)$$

$$F_{\mu\nu}^a = \partial_{\mu} A_{\nu}^a - \partial_{\nu} A_{\mu}^a - gf_{abc} A_{\mu}^b A_{\nu}^c. \quad (5)$$

Here q , $\vec{\phi}$, A_μ^a and χ are the quark, pion, gluon, and dielectric fields respectively, $\kappa(\chi)$ is the dielectric coefficient (other CDM models may have different functional forms for $\kappa(\chi)$), $F_{\mu\nu}^a$ is the gluon field tensor, $\vec{\tau}$ is the isospin operator of the pion, λ_a and f_{abc} are Gell-Mann matrices and SU(3) structure constants, m_q and m_π are the quark and pion masses, and $D_\mu\vec{\phi}$ is the covariant derivative of the pion field. Arrows over quantities denote their isovector nature. The form (2) of the Lagrangian becomes invariant under chiral transformations when the pion mass is set equal to zero.

An important, yet phenomenological, part of the CDM Lagrangian (2) is the dielectric self-interaction field $U(\chi)$. We express it in terms of the bag constant B , a shape parameter α , and the dielectric field χ :

$$U(\chi) = B\alpha\chi^2 \left[1 - 2 \left(1 - \frac{2}{\alpha} \right) \chi + \left(1 - \frac{3}{\alpha} \right) \chi^2 \right]. \quad (6)$$

This self-interaction field has an absolute minimum when the dielectric field $\chi = 0$ and $\alpha > 6$, and has a local minimum when $\chi = 1$. Of particular importance is the behavior of the Lagrangian (2) in the limit of vanishing dielectric field, $\chi \rightarrow 0$. In this limit, the gluon kinetic energy term $\chi^4 F^2/4$ vanishes and the quark effective mass m_q/χ becomes infinite. Accordingly, we have the distinguishing characteristic of the CDM: the quark and gluon fields are confined within the baryon to the region of non-vanishing dielectric field χ . This contrasts with the bag model in which confinement is externally imposed by placing the quarks within an infinite square well.

As we see from the form of the Lagrangian (2) with the dielectric self-interaction field (6), the CDM has five parameters: the quark mass m_q , the strong coupling constant g (or equivalently $\alpha_s = g^2/4\pi$), the pion decay constant f , the glueball (or dielectric field) mass $m_{gb} \equiv \sqrt{2B\alpha}/\sigma_v$, and the bag constant B . Although we do adjust some of these parameters to experimental data, their values are far from arbitrary. For example, the glueball mass m_{gb} essentially sets the scale of energy, and the values of the coupling and decay constants must be close to the accepted values for the model to be considered realistic.

A. Pseudo-vector Coupling

In order for the Weinberg-Tomozawa relation to appear explicitly in S-wave π N scattering at the tree level (and thus guarantee that the Born approximation scattering lengths are reasonable), we perform a unitary transformation [4] on the quark fields, $q \rightarrow \exp[i\gamma_5 \vec{\tau} \cdot \vec{\phi}/(2f)]q$. This transforms the original CDM Lagrangian (2) to

$$\begin{aligned} \mathcal{L} = & \bar{q} \left[i\gamma^\mu D_\mu - \frac{m_q}{\chi} + \frac{1}{2f} \gamma^\mu \gamma_5 \vec{\tau} \cdot D_\mu \vec{\phi} - \frac{g}{2} \lambda_a \gamma^\mu A_\mu^a \right] q \\ & - \frac{\kappa(\chi)}{4} (F_{\mu\nu}^a)^2 + \frac{\sigma_v^2}{2} (\partial_\mu \chi)^2 - U(\chi) + \frac{(D_\mu \vec{\phi})^2}{2} - \frac{m_\pi^2 \vec{\phi}^2}{2}, \end{aligned} \quad (7)$$

where the covariant derivative on the quark fields are defined as

$$D_\mu q = \partial_\mu q - \frac{i}{2} \left(\cos \frac{\phi}{f} - 1 \right) \vec{\tau} \cdot \hat{\phi} \times \partial_\mu \hat{\phi} q. \quad (8)$$

These new quark fields are dressed by the pions. We next expand the Lagrangian in powers of the inverse of f , and retain terms up to order $1/f^2$. We separate off terms linear and quadratic in $1/f$ and identify them as the interaction Hamiltonian:

$$H_{int} \simeq H_{1\pi} + H_{2\pi}, \quad (9)$$

where

$$H_{1\pi} = -\frac{1}{2f} \int d^3x \bar{q} \gamma^\mu \gamma_5 \vec{\tau} q \cdot \partial_\mu \vec{\phi}, \quad (10)$$

$$H_{2\pi} = \frac{1}{4f^2} \int d^3x \bar{q} \gamma^\mu \vec{\tau} q \cdot \vec{\phi} \times \partial_\mu \vec{\phi}. \quad (11)$$

These elementary vertices are illustrated in Figure 1. You will notice that the one-pion vertex $H_{1\pi}$ has a pseudovector coupling between the pion and the quark. The only surviving term for S-wave scattering is the two-pion contact interaction $H_{2\pi}$ which comes from the covariant derivative on quarks; this term reproduces the Weinberg-Tomozawa result which was originally derived from current algebra.

Both the scalar dielectric field and the screened gluon fields exist in the Lagrangian (7). The simplest treatment of them is in a mean field approximation in which we ignore the

screened gluon fields and the pion clouds (one then needs one-gluon-exchange “corrections” to split the nucleon and delta masses). Pions are included perturbatively in the theory as we derive the bare vertex function and later dress the bare vertices by means of the Lippmann-Schwinger equation (1).

B. Vertex Functions with the Static Baryons

The equations of motion for the static quark and dielectric fields in MFA are:

$$\left(i\gamma^\mu\partial_\mu - \frac{m_q}{\chi}\right)q = 0, \quad (12)$$

$$\sigma_v^2\partial_\mu\partial^\mu\chi + \frac{dU(\chi)}{d\chi} - \frac{m_q}{\chi^2}\bar{q}q = 0. \quad (13)$$

These are coupled, nonlinear, partial differential equations. We solve them numerically for χ 's with soliton-like behaviors. For bare N and Δ , all valence quarks are in $1S$ state, and so the quark wave function is assumed to be

$$q(x) = \frac{N_s}{\sqrt{4\pi}} \begin{pmatrix} g(r) \\ i\sigma \cdot \hat{r}f(r) \end{pmatrix} \xi_{s\mu} e^{-i\omega_s t}, \quad (14)$$

where $\xi_{s\mu}$ is the quark spin wave function. As usual, the scalar-isoscalar dielectric field χ is assumed to be time-independent and spherically symmetric.

In the same spirit as the cloudy bag model, we treat the baryons as composite, three quark systems, while simultaneously treating the pions as an elementary, quantized fields. As illustrated in Figure 1, the interaction hadron-space Hamiltonian involving a single pion is then:

$$H_{1\pi}^B = \sum_{\alpha,\beta} B_\beta^\dagger B_\alpha \int \frac{d^3k k_\mu}{(2\pi)^{3/2}} [\vec{a}(k) \cdot \vec{\mathcal{V}}_{\beta\alpha}^\mu(\mathbf{k}) + \text{h.c.}], \quad (15)$$

where h.c. denotes Hermitian conjugate, $\vec{a}(k)$ is the pion annihilation operator, and the vertex function $\vec{\mathcal{V}}_{\beta\alpha}^\mu$ is the matrix element of the quark pseudovector current evaluated between transition baryon states:

$$\vec{\mathcal{V}}_{\beta\alpha}^\mu(\mathbf{k}) = -\frac{i}{2f} \int d^3x \frac{e^{i\mathbf{k}\cdot\mathbf{x}} \langle B_\beta | \bar{q} \gamma^\mu \gamma_5 \vec{\tau} q | B_\alpha \rangle}{\sqrt{(2\pi)^3} 2\omega_\pi(k)} \quad (16)$$

$$= -\frac{i}{2f} \frac{u^{PV}(k) \langle B_\beta | \sigma \cdot \hat{\mathbf{k}} \vec{\tau} | B_\alpha \rangle^{sf}}{\sqrt{(2\pi)^3} 2\omega_\pi(k)}. \quad (17)$$

The function $u^{PV}(k)$ in (17) is the π NN pseudovector form factor defined in the Appendix. The bracket in (17) is a spin-flavor matrix element which we reduce via the Wigner-Eckart theorem:

$$\begin{aligned} \langle B_\beta | \sigma \cdot \hat{\mathbf{k}} \vec{\tau} | B_\alpha \rangle^{sf} &= -\sqrt{\frac{4\pi}{3}} \sum_M Y_{1M}^*(\hat{k}) \lambda_{B_\alpha M B_\beta} \\ &\times C_{\mu M \mu_{B_\beta}}^{s_B 1 s_{B_\beta}} C_{i_B i_M i_{B_\beta}}^{I_B I_M I_{B_\beta}}, \end{aligned} \quad (18)$$

where $C_{\mu M \mu_{B_\beta}}^{s_B 1 s_{B_\beta}}$ and $C_{i_B i_M i_{B_\beta}}^{I_B I_M I_{B_\beta}}$ are Clebsch-Gordon coefficients and the $\lambda_{B_\alpha M B_\beta}$ are the one-pion coupling constants given in Table I.

The contact interaction directly couples the initial pion and baryon to the final pion and baryon, Figure 1, and takes the form:

$$\begin{aligned} H_{2\pi}^B &= \sum_{\alpha,\beta} B_\beta^\dagger B_\alpha \int \frac{d^3k d^3k'}{(2\pi)^3} \\ &\times \left[(\vec{a}^\dagger(k') \times k_\mu \vec{a}(k)) \cdot \vec{\mathcal{W}}_{\beta\alpha}^\mu(\mathbf{k}', \mathbf{k}) + \text{h.c.} \right]. \end{aligned} \quad (19)$$

We evaluate the time and space components of the contact interaction separately:

$$\begin{aligned} \vec{\mathcal{W}}_{\beta\alpha}^T(\mathbf{k}', \mathbf{k}) &= \frac{\omega_\pi(k) + \omega_\pi(k')}{4\pi^2 f^2 \sqrt{4\omega_\pi(k)\omega_\pi(k')}} \sum_{LM} Y_{LM}^*(\hat{k}') Y_{LM}(\hat{k}) \\ &\times v_L^{CT}(k', k) \langle B_\beta | -\frac{i}{2} \epsilon_{ijk} \tau_i | B_\alpha \rangle^{sf}, \end{aligned} \quad (20)$$

$$\begin{aligned} \vec{\mathcal{W}}_{\beta\alpha}^S(\mathbf{k}', \mathbf{k}) &= \frac{1}{4\pi^2 f^2 \sqrt{4\omega_\pi(k)\omega_\pi(k')}} \sum_{JLMM'} Y_{LM}^*(\hat{k}') Y_{LM}(\hat{k}) \\ &\times C_{\mu' m' j}^{S' L J} C_{\mu M J}^{S L J} A^{JLS} v_L^{CS}(k', k) \langle B_\beta | \frac{-i}{2\sqrt{6}} \epsilon_{ijk} \tau_i \sigma | B_\alpha \rangle^{sf}, \end{aligned} \quad (21)$$

$$A^{JLS} = -2\sqrt{6} \langle L \parallel \mathbf{L} \parallel L \rangle (-)^{J+S+L} \begin{Bmatrix} S' & S & 1 \\ L & L & J \end{Bmatrix}. \quad (22)$$

The spin-flavor matrix elements are

$$\left\langle B_\beta \left| -\frac{i\epsilon_{ijk}}{2}\tau_i \right| B_\alpha \right\rangle^{sf} = \sum_I \lambda_{\beta\alpha}^{TI} C_{i_B i_{M'}^I}^{I_B I_M^I} C_{i_{B'} i_{M'}^I}^{I_{B'} I_{M'}^I}, \quad (23)$$

$$\left\langle B_\beta \left| -\frac{i\epsilon_{ijk}}{2\sqrt{6}}\tau_i\sigma \right| B_\alpha \right\rangle^{sf} = \sum_I \lambda_{\beta\alpha}^{SI} C_{i_B i_{M'}^I}^{I_B I_M^I} C_{i_{B'} i_{M'}^I}^{I_{B'} I_{M'}^I}, \quad (24)$$

where the two-pion coupling constants $\lambda_{\beta\alpha}^{TI}$ and $\lambda_{\beta\alpha}^{SI}$ are given in Table II. In the Appendix, the vertex functions $v_L^{CT}(k', k)$ and $v_L^{CS}(k', k)$ are related to the nucleon electromagnetic form factors.

C. Vertex Functions with Momentum-Projected Baryons

The solutions of equations (12)-(13) describe quark orbits within baryons in which the COM may move. While this may not be too serious a concern for bound-state spectra, it is for scattering where the large momentum transfers make recoil effects important. We remove this spurious motion by a Peierls-Yoccoz [12] projection to form an eigenstate of momentum \mathbf{p} :

$$|B(\mathbf{p})\rangle = \frac{1}{N_B} \int d\mathbf{r} e^{i\mathbf{p}\cdot\mathbf{r}} q_{\mathbf{r}}^\dagger q_{\mathbf{r}}^\dagger q_{\mathbf{r}}^\dagger |C_{\mathbf{r}}\rangle, \quad (25)$$

where N_B is a momentum-dependent normalization constant. The operator $q_{\mathbf{r}}^\dagger$ creates a quark at point \mathbf{r} . The ket $|C_{\mathbf{r}}\rangle$ represents the coherent state of the dielectric field generated from the mean field solution [3]:

$$|C_{\mathbf{r}}\rangle = \exp \left[\int d^3k \sqrt{\omega(k)/2} f_{\mathbf{r}}(\mathbf{k}) a_{gb}^\dagger(\mathbf{k}) \right] |0\rangle. \quad (26)$$

In (26), $|0\rangle$ is the vacuum state, $f_{\mathbf{r}}(\mathbf{k})$ is the Fourier transform of the scalar dielectric field $\chi(\mathbf{r})$, and $a_{gb}^\dagger(\mathbf{k})$ is the creation operator for a scalar dielectric field quanta with energy $\omega(k) = \sqrt{m_{gb}^2 + k^2}$. Accordingly, the pseudovector vertex function with recoil corrections is evaluated between the momentum-projected baryon states in the Breit frame:

$$\vec{V}_{\beta\alpha}^\mu(\mathbf{k}) = \frac{-i \left\langle B_\beta(-\frac{\mathbf{k}}{2}) \left| \bar{q}(0) \gamma^\mu \gamma_5 \vec{\tau} q(0) \right| B_\alpha(\frac{\mathbf{k}}{2}) \right\rangle}{2f \sqrt{2\omega_\pi(k)}}. \quad (27)$$

After making these same projections and evaluations, the corresponding contact interaction Hamiltonian (11) takes the form:

$$\vec{\mathcal{W}}_{\beta\alpha}^{\mu}(\mathbf{q}) = \frac{\langle B_{\beta}(-\frac{\mathbf{q}}{2}) | \bar{q}(0) \gamma^{\mu} \vec{\tau} q(0) | B_{\alpha}(\frac{\mathbf{q}}{2}) \rangle}{4f^2 \sqrt{4\omega_{\pi}(k)\omega_{\pi}(k')}}}, \quad (28)$$

where $\mathbf{q} = \mathbf{k}' - \mathbf{k}$ is the momentum transfer. Detailed expressions for the vertex functions are given in the Appendix.

The vertex function $\vec{\mathcal{V}}_{\beta\alpha}^i(k)$ is of some interest in its own right because it is related to the axial form factor of the nucleon. In particular, $\mathcal{V}_{N,N}(k)$ in the $k \rightarrow 0$ limit determines g_A of nucleon. We find in our calculations that g_A calculated using momentum-projected states is larger than that calculated statically. Similar behavior is expected for other meson-baryon coupling constants. The form factor $\vec{\mathcal{W}}_{\beta\alpha}^{\mu}(q)$ for the contact interaction is the matrix element of the vector current, and has time and space components which are proportional to the charge and magnetic form factors of the baryons.

D. One Gluon Exchange Corrections

While it is good that we have been able to solve the field equations in the mean field approximation, the approximations involved leave the nucleon and delta with the same mass. This degeneracy is removed by including one gluon exchange corrections. Since the scalar dielectric field χ is responsible for the confinement of gluons, it is consistent to ignore the self-interaction of the residual gluon. This means we drop the non-Abelian $gf_{abc}A_{\mu}^b A_{\nu}^c$ term in equation (5) for the gluon field tensor $F^{a,\mu\nu}$. Under the Coulomb gauge condition $\nabla \cdot (\kappa \mathbf{A}^a) = 0$, the equations for the time and space components of the gluon fields become,

$$-\nabla \cdot (\kappa \nabla A^{a,0}) = j^{a,0} \quad (29)$$

$$\kappa \partial_0^2 \vec{A}^a - \nabla^2 (\kappa \mathbf{A}^a) + \nabla \times (\kappa \mathbf{A}^a \times \nabla \ln \kappa) = \mathbf{j}_t^a \quad (30)$$

Here $j^{a,\nu} = \frac{1}{2} g \bar{q} \gamma^{\nu} \lambda^a q$ is the quark current, and \mathbf{j}_t^a is its transverse component. We follow Bickeboller et al. [13] and solve these equations for A_{μ}^a with Green's function techniques. As is done in bag model calculations [2], the contribution of the gluon electric energy is neglected. The gluon magnetic energy can then be expressed in the form:

$$E_{mag} = \left\langle B(0) \left| \sum_{a,i < j} \mathbf{A}^a(i) \cdot \mathbf{j}^a(j) \right| B(0) \right\rangle, \quad (31)$$

where $\mathbf{A}^a(i)$ is the gluon field due to i -th quark. The bare baryon mass is the sum of the expectation values of the bare Hamiltonian for a zero-momentum baryon state plus the gluon magnetic energy:

$$m_{B_0}^{(0)} = \langle B(0) | H_{bare} | B(0) \rangle + E_{mag}, \quad (32)$$

$$H_{bare} = \int d^3x \left[\sum_i q_i^\dagger \left(-i\boldsymbol{\alpha} \cdot \nabla + \frac{\gamma^0 m_q}{\chi} \right) q_i + \frac{\sigma_v^2}{2} \{ (\nabla\chi)^2 + \pi^2 \} + U(\chi) \right], \quad (33)$$

where π is the conjugate momentum of the χ field. When these steps are followed, the masses of the bare nucleon and delta can be written as

$$m_N^{(0)} = m_{gb}(C_1 - \alpha_s C_2), \quad (34)$$

$$m_\Delta^{(0)} = m_{gb}(C_1 + \alpha_s C_2), \quad (35)$$

where C_1 and C_2 are constants determined from the mean field solutions.

III. UNITARY

In the present work we concentrate on πN scattering in the energy region from threshold through the Δ resonance. Even though the $\pi\Delta$ channel is closed for these energies, we include coupling to an explicit $\pi\Delta$ channel in order to include its effect on πN scattering and to permit a subsequent extension of the theory to Δ production. To ensure unitarity we iterate the tree-level diagrams using the relativistic Lippmann-Schwinger equation (1). The resulting T matrices have the desired renormalized poles together with the pion-dressed vertex functions. In Figure 2 we show the three distinct terms which contribute in lowest order to the πN and $\pi\Delta$ potentials:

1. **Direct Born term**, Figure 2a. This part of the potential arises from two elementary vertices connected by an intermediate bare baryon state B_0 . In the partial-wave basis,

$$\begin{aligned}
V_{\beta\alpha}^{(a)LJI}(k', k) &= \frac{\delta_{II_{B_0}} \delta_{JJ_{B_0}} \delta_{L1} k' k}{48\pi f^2 \sqrt{4\omega_\pi(k)\omega_\pi(k')}} \\
&\times \sum_{B_0} \lambda_{B'M'B_0} \lambda_{BMB_0} \frac{u^{PV}(k') u^{PV}(k)}{E - m_{B_0}^{(0)}}.
\end{aligned} \tag{36}$$

Here E is the COM energy and $m_{B_0}^{(0)}$ is the bare mass of the intermediate nucleon or delta. Spin and isospin conservation restricts the intermediate state to the P_{11} and P_{33} channels.

2. **Crossed Born term**, Figure 2b. This term arises from crossing the external pion lines of the pole diagram. Since the intermediate state contains two pions and one baryon, this modifies the propagator and so:

$$\begin{aligned}
V_{\beta\alpha}^{(b)LJI}(k', k) &= \frac{\delta_{L1} k' k}{48\pi f^2 \sqrt{4\omega_\pi(k)\omega_\pi(k')}} \\
&\times \sum_{B_0} \lambda_{B_0MB'} \lambda_{B_0M'B} \frac{\eta_{\beta\alpha}^{LJI} u^{PV}(k') u^{PV}(k)}{E - m_{B_0}^{(0)} - \omega_\pi(k) - \omega_\pi(k')}.
\end{aligned} \tag{37}$$

The spin-isospin coefficient is defined as

$$\begin{aligned}
\eta_{\beta\alpha}^{LJI} &= (-1)^{S_B+S_{B'}+I_B+I_{B'}+I_M+I_{M'}} \hat{S}_B \hat{S}_{B'} \hat{I}_B \hat{I}_{B'} \\
&\times \begin{Bmatrix} I_M & I_B & I \\ I_{M'} & I_{B'} & I_{B_0} \end{Bmatrix} \begin{Bmatrix} S_B & 1 & J \\ S_{B'} & 1 & S_{B_0} \end{Bmatrix}.
\end{aligned} \tag{38}$$

Recoil of the intermediate baryons are ignored in our calculations, and thus the crossed term contributes only to P-wave πN scattering.

3. **Contact term**, Figure 2c. The contact term arises from $H_{2\pi}$, the two-pion vertex of the interaction Hamiltonian. This term gives rise to two potentials, $V_{\beta\alpha}^{CT}$ due to the time component, and $V_{\beta\alpha}^{CS}$ due to the space component. In the partial-wave basis,

$$V_{\beta\alpha}^{(CT)LJI}(k', k) = \frac{(\omega_\pi(k) + \omega_\pi(k')) \lambda_{\beta\alpha}^{TI} v_L^{CT}(k', k)}{8\pi f^2 \sqrt{4\omega_\pi(k)\omega_\pi(k')}} \tag{39}$$

$$V_{\beta\alpha}^{(CS)LJI}(k', k) = \frac{\lambda_{\beta\alpha}^{SI} A^{JLS} v_L^{CS}(k', k)}{8\pi f^2 \sqrt{4\omega_\pi(k)\omega_\pi(k')}} \tag{40}$$

where A^{JLS} has been defined previously (22), and the spin-flavor coupling constants are given in Table II.

IV. RESULTS

We have used a CDM to generate the potential terms for the relativistic Lippmann-Schwinger equation (1). The pion interaction resulting from the iteration of the potential by the Lippmann-Schwinger equation ensures two body unitarity of T and renormalizes the $\pi\text{BB}'$ vertex and the bare baryon masses. The energies of the poles of T are identified with renormalized masses for the physical states, the residues of the poles are identified with renormalized coupling constants, and the momentum distributions around the poles are related to the form factors.

When fitting data we always start off with a value for the glueball mass $m_{gb} \simeq 1$ GeV. The precise value does not appear to be important, but its general magnitude does set the energy scale in the equations of motion. We keep the shape parameter of the self-interaction of dielectric field fixed at $\alpha = 24$ since previous studies with the pseudoscalar version of the CDM [10] have shown that the static properties of baryons are insensitive to α for this size of m_{gb} . Each time we obtain a solution of the field equations, we adjust the parameters m_{gb} , α_s , and f to best describe the πN phase shifts and the masses of the nucleon and delta. Somewhat surprisingly, we found that we can reproduce the experimental masses for a large range of quark masses and bag constants just by adjusting the values for m_{gb} and α_s . Specifically, we find that we can vary the bag constant $B^{1/4}$ between 100 MeV and 150 MeV, and the quark mass between 40 MeV and 120 MeV. While 40 MeV may appear small, the dielectric field also becomes small near the origin (the “one phase” solution in which the wave function has no abrupt phase transition). Consequently, the 40 MeV quark has an effective mass inside of a nucleon of $m_q/\chi(r \simeq 0) \simeq 100$ MeV.

The fitted parameters and deduced bare masses are given in Table III. The value $f = 93$ MeV for the pion decay constant is the accepted value [14], and the value $f = 90$ MeV is very close. Our value $\alpha_s \simeq 0.12$ for the quark-gluon coupling constant is much smaller than the MIT bag result, $\alpha_s \simeq 2.2$ [15] or the favored value in the Friedberg-Lee model. In fact Bickeboller et al. [13] have found that α_s can vary over two orders of magnitude depending

on the choice of the dielectric coefficient and the parameters of the self-interaction of the dielectric field. In our case, a small value of α_s compensates for our model of the dielectric field, $\kappa(\chi) = \chi^4$, which otherwise would produce too large a color-magnetic energy. In addition, the pion-dressing in our model makes up for part of the N and Δ mass difference. This also makes the value of α_s , which measures the strength of OGE in our model, smaller than in those models without dressing. Our fitted value $m_{gb} \simeq 1153 \text{ MeV}$ for the glueball mass is consistent with the values found in other models [3], and is in the region where glueball may occur [16]. Finally, we see in Table III that the effect of renormalization on the nucleon and delta masses is to move the bare masses down by $\sim 250 \text{ MeV}$. Our calculation of scattering lengths indicates the need for some additional repulsion in our model, and we suspect that that repulsion would lead to less mass renormalization.

A. Coupling Constants, Masses, and Form Factors

As indicated in (11), we have deduced the CDM Hamiltonians $H_{1\pi}$ and $H_{2\pi}$ from an expansion of the Lagrangian in inverse powers of the pion's weak decay constant f , or equivalently, as a series expansion in the πNN coupling constant $f_{\pi NN}$. This equivalence follows from the Goldberger-Trieman relation [4]:

$$\frac{1}{2f} = \sqrt{4\pi} \frac{f_{\pi NN}}{m_\pi}. \quad (41)$$

While the relation (41) relates the bare coupling constants, our study also produces renormalized coupling constants. We extract the bare coupling constant $f_{\pi NN}^{(0)}$ from our final T by comparing the vertex function computed with the CDM to that of standard Chew-Low theory [4]:

$$v_i(k) = i\sqrt{\frac{4\pi}{2\omega_k}} \frac{f_{\pi NN}^{(0)}}{m_\pi} g(k) \tau_i \sigma \cdot \mathbf{k}. \quad (42)$$

We then extract the renormalized πNN coupling constant $f_{\pi NN}$ and the renormalized $\pi N\Delta$ coupling constant $f_{\pi N\Delta}$ by making Laurent expansions of the computed T matrix around its poles:

$$\hat{T}(k', k; E \simeq m_N) \simeq f_{\pi NN}^2 \frac{g_{\pi NN}(k')g_{\pi NN}(k)}{E - m_N} + \dots, \quad (43)$$

$$\hat{T}(k', k; E \simeq m_\Delta) \simeq f_{\pi N\Delta}^2 \frac{g_{\pi N\Delta}(k')g_{\pi N\Delta}(k)}{E - m_\Delta} + \dots. \quad (44)$$

This expansion permits us to deduce not only coupling constants but also the πNN and $\pi N\Delta$ form factors $g_{\pi NN}(k)$ and $g_{\pi N\Delta}(k)$ from the momentum dependence of the T matrices in (43) and (44). It is particularly interesting to compare these form factors with those calculated in other approaches since the form factors are related to the CDM quark wave functions (which should be fairly realistic), and since they are affected by the renormalization process.

While we have already indicated that fits to the data do not determine a unique set of parameters, the different parameter sets are correlated. In the upper part of Figure 3 we show the relation between the strong coupling constant $f_{\pi NN}$ deduced from our fits and the bare, weak decay constant f (note the false origin). The dashed curve relates the bare values of $f_{\pi NN}$ as determined from the Goldberger-Trieman relation (41), or equivalently, from the potential directly. The solid curve relates the renormalized values determined via (43). We see that there is a similar functional dependence in each case with an $\sim 15\%$ renormalization effect.

Although not shown in the figure, we have also calculated $f_{\pi N\Delta}$ from the residue of the Δ pole and find:

$$\frac{f_{\pi N\Delta}}{f_{\pi NN}} \simeq 1.87. \quad (45)$$

This ratio is quite close to the experimental value of ~ 2 , closer in fact than the SU(6) prediction [4] of $6\sqrt{2}/5 \simeq 1.70$. This clearly shows the importance of renormalization.

In the lower part of Figure 4 we show the πNN form factors deduced from the behavior of the T matrix near the nucleon pole. The two different curves correspond to two different values of the pion decay constant f . One can estimate from the falloff that the range $R \simeq 0.5\text{fm}$. To compare with other models which have a monopole form factor, we assume

$$g(k \rightarrow 0) \simeq \frac{1}{1 + k^2 R^2}, \quad (46)$$

$$\Rightarrow R = \lim_{k \rightarrow 0} \sqrt{\frac{g'(k)}{-2k}} = \begin{cases} 0.47 \text{ fm} & f = 90 \text{ MeV}, \\ 0.48 \text{ fm} & f = 93 \text{ MeV}. \end{cases} \quad (47)$$

This R is comparable with the value $R \simeq R_{\text{bag}}/\sqrt{10}$ obtained from the cloudy bag model with a bag radius $R_{\text{bag}} \simeq 1 \text{ fm}$. The meson exchange models, however, use much smaller $R \sim 0.15 \text{ fm}$ which produces a much harder form factor.* In practice, a monopole form factor falls off much slower than the form factor calculated in our model. If we replace our form factor with the monopole form factor defined above and use it in an actual T-matrix calculation, we would get poor agreement with the experimental phase shifts. Thus, in contrast to the meson exchange models, pion-nucleon scattering seems to require soft form factors like the ones obtained in our model. A similar conclusion has also been reached recently by others [17].

B. S and P Wave Phase Shifts

In Figure 5 we compare the low-energy S- and P-wave phase shifts calculated with the CDM model to the experimental phases obtained from the *said* analysis [18]. The solid and dashed curves are for parameter sets with $f=90 \text{ MeV}$ and $f=93 \text{ MeV}$ respectively. In Table IV a comparison of just the scattering lengths is given. We see excellent agreement in the P_{33} channel, with the energy of the delta and its width reproduced well. The small P-wave phases are always more of a challenge. The scattering volumes for the P_{31} and P_{13} channels are predicted well, with the calculated energy dependence in the P_{31} phase very similar to the data. In Table IV we give values for the scattering lengths calculated in Born approximation, that is, when only the potential term in the Lippmann-Schwinger equation (1) is used for T . As expected, these values agree with the chiral limits:

$$a_1 = \frac{\mu}{4\pi f^2}, \quad a_3 = -\frac{\mu}{8\pi f^2}, \quad (48)$$

*We remind the reader that the monopole approximation (46) is for comparison only and that this radius is determined from the behavior of the form factor in the $k \rightarrow 0$ limit.

where μ is the π N reduced mass. Comparison of the Born results to experiment and to our full calculation indicates that renormalization is large, and that some additional repulsion is needed.

The P_{11} channel is a particular problem for simple models like ours. Increasing the agreement with the P_{33} phases decreases the agreement with the P_{11} phases. We have assumed that the Roper(1440) is a $(1s)^2(2s)$ three-quark state, and included it as an intermediate state for both s- and u-channel diagrams. The results show that the elementary Roper does provide the attraction needed for the phase shift to change sign from negative to positive, but does not do much to improve the fit at lower energies. In addition, we find that the P_{11} amplitude does not have the desired pole at the physical Roper resonance unless we introduce extra, free parameters. Indeed, the calculations of Elsey and Afnan [19] and Pearce and Afnan [20] indicate that the coupling of three-body ($\pi\pi$ N) channels is important, as are some $1/f^4$ diagrams not present in our calculation. These should be included in the continuation of the present work.

As is true for the small P-wave phases, the predicted S-wave phase shift shown in Figure 5 show the need for additional repulsion. Cooper and Jennings [21] indicate that agreement may require the inclusion of certain $1/f^4$ graphs which cancel at $m_\pi = 0$ but produce repulsion for $m_\pi > 0$.

V. SUMMARY AND CONCLUSION

We have studied low-energy π N elastic scattering in a chiral version of the color dielectric model. Our calculations are similar to those done with the cloudy bag model [6]. Our major improvement is a more natural and realistic inclusion of quark confinement, the inclusion of baryon-recoil effects, and the coupling of the π N and $\pi\Delta$ channels. The CDM is used to derive effective potentials containing terms up to second order in the π NN coupling, and these potentials are used as input to relativistic, coupled-channel Lippmann-Schwinger equations. The model reproduces the physical nucleon and delta masses, and then predicts

the π NN and π N Δ coupling constants and form factors, and low-energy π N scattering.

We find much success for such a simple model. Specifically, we can simultaneously obtain the correct renormalized masses for the nucleon and delta, the correct delta width, the π NN coupling constant to within 5% of its experimental value, the ratio of the renormalized π N Δ to π NN coupling constants which is better than the SU(6) value, excellent agreement with the P_{33} phase shifts from threshold through the delta resonance energy, good agreement with the P_{13} and P_{31} scattering volumes, and good agreement with the energy dependence of the P_{31} phase shift for the first 300 MeV of kinetic energy. Better agreement with the S-wave and small P-wave phases requires additional repulsion in the model, possibly obtained by one-loop corrections. The model could also be improved by obtaining solutions to the field equations beyond those of the mean field approximation and by the inclusion of additional dielectric fields [22].

APPENDIX: FORM FACTORS FOR π N SCATTERING

We give here the complete form factors for the $(\pi$ N, π Δ) system. Since the Δ differs from the N only in spin-isospin orientations, they have the same space wave function and thus the same form factors. The pseudovector vertex functions with the momentum projected states evaluated in the Breit frame are:

$$\begin{aligned}
\vec{V}_{\beta\alpha}^{\mu}(\mathbf{k}) &= -\frac{i \langle B_{\beta}(-\frac{\mathbf{k}}{2}) | \bar{q}(0) \gamma^{\mu} \gamma_5 \vec{\tau} q(0) | B_{\alpha}(\frac{\mathbf{k}}{2}) \rangle}{2f \sqrt{2\omega_{\pi}(k)}} \\
&= \frac{-i \int d\mathbf{x} d\mathbf{y} e^{-i\mathbf{k}\cdot(\mathbf{x}+\mathbf{y})/2} \langle B_{\beta} | \bar{q}(0) \gamma^{\mu} \gamma_5 \vec{\tau} q(0) | B_{\alpha} \rangle_{\mathbf{x}}}{2f \sqrt{2\omega_{\pi}(k)} N_{B_{\beta}} N_{B_{\alpha}}} \\
&= \frac{i}{2f \sqrt{2\omega_{\pi}(k)}} u^{PV}(k) \langle B_{\beta} | \sigma \cdot \hat{\mathbf{k}} \vec{\tau} | B_{\alpha} \rangle^{sf}. \tag{A1}
\end{aligned}$$

Where $N_{B_{\alpha}} = \sqrt{\langle B_{\alpha}(\frac{\mathbf{k}}{2}) | B_{\alpha}(\frac{\mathbf{k}}{2}) \rangle}$ is a momentum-dependent normalization constant for a projected baryon state, and $|B_{\alpha}\rangle_{\mathbf{x}} = q_{\mathbf{x}}^{\dagger} q_{\mathbf{x}}^{\dagger} q_{\mathbf{x}}^{\dagger} |C_{\mathbf{x}}\rangle$ is a localized baryon state. The pseudovector form factor has the form, $u^{PV}(k) = N(k)/D(k)$, with

$$N(k) = \int z^2 dz N_q^2(z) N_\chi(z) \int d^3 r \times \left\{ g_+ g_- j_0(kr) - \frac{f_- f_+}{3r_- r_+} \left[[j_0(kr) + 4j_2(kr)] r^2 - [j_0(kr) + 4j_2(kr) P_2(\hat{r} \cdot \hat{z})] \frac{z^2}{4} \right] \right\}, \quad (\text{A2})$$

$$D(k) = \int z^2 dz j_0(kz/2) N_q^3(z) N_\chi(z), \quad (\text{A3})$$

$$N_q(z) = \int d^3 r \left[g_+ g_- + \frac{f_+ f_-}{r_+ r_-} \left(r^2 - \frac{z^2}{4} \right) \right], \quad (\text{A4})$$

$$N_\chi(z) = \exp \left[2\pi \int k^2 dk \omega(k) |f_0(k)|^2 j_0(kz) \right]. \quad (\text{A5})$$

In the above equations, we have defined $r_\pm = |\mathbf{r} \pm \mathbf{z}/2|$, $g_\pm = g(r_\pm)$, and $f_\pm = f(r_\pm)$. The function $f_0(k)$ is the Fourier transform of the mean field solution of the classical dielectric field. Without the COM correction, $g_\pm = g(r)$, $f_\pm = f(r)$, and the π NN pseudovector form factor is reduced to the static limit:

$$u^{PV}(k) = N_s^2 \int r^2 dr \left\{ \left[g(r)^2 - \frac{f^2(r)}{3} \right] j_0(kr) - \frac{4f^2(r)}{3} j_2(kr) \right\}. \quad (\text{A6})$$

The vertex functions for the contact interaction are

$$\begin{aligned} \vec{\mathcal{W}}_{\beta\alpha}^\mu(\mathbf{q}) &= \frac{1}{8f^2 \sqrt{\omega_\pi(k)\omega_\pi(k')}} \left\langle B_\beta(-\frac{\mathbf{q}}{2}) \left| \vec{q}(0) \gamma^\mu \vec{\tau} q(0) \right| B_\alpha(\frac{\mathbf{q}}{2}) \right\rangle \\ &= \frac{1}{8f^2 \sqrt{\omega_\pi(k)\omega_\pi(k')} N_{B_\beta} N_{B_\alpha}} \\ &\quad \times \int d\mathbf{x} d\mathbf{y} e^{-i\mathbf{q} \cdot (\mathbf{x}+\mathbf{y})/2} \langle B_\beta | \vec{q}(0) \gamma^\mu \vec{\tau} q(0) | B_\alpha \rangle_{\mathbf{x}} \\ &= \frac{1}{8f^2 \sqrt{\omega_\pi(k)\omega_\pi(k')}} \\ &\quad \times \begin{cases} u^{CT}(q) \langle B_\beta | \vec{\tau} | B_\alpha \rangle^{sf}, & \text{time,} \\ u^{CS}(q) \langle B_\beta | -\sigma \times \hat{\mathbf{q}} \vec{\tau} | B_\alpha \rangle^{sf}, & \text{space.} \end{cases} \end{aligned} \quad (\text{A7})$$

The form factors for the time and space components are respectively:

$$u^{CT}(q) = \frac{N^{CT}(q)}{D(q)}, \quad u^{CS}(q) = \frac{N^{CS}(q)}{D(q)}, \quad (\text{A8})$$

$$\begin{aligned} N^{CT}(q) &= N_s^2 \int z^2 dz N_q^2(z) N_\chi(z) \int d^3 r j_0(qr) \\ &\quad \times \left[g_+ g_- + \left(r^2 - \frac{z^2}{4} \right) \frac{f_+ f_-}{r_+ r_-} \right], \end{aligned} \quad (\text{A9})$$

$$\begin{aligned}
N^{CS}(q) &= N_s^2 \int z^2 dz N_q^2(z) N_\chi(z) \int d^3 r \frac{j_1(qr)}{qr} \\
&\times \left[r^2 \left(\frac{g_+ f_-}{r_-} + \frac{g_- f_+}{r_+} \right) - \frac{\hat{r} \cdot \hat{z}}{2} \left(\frac{g_+ f_-}{r_-} - \frac{g_- f_+}{r_+} \right) \right].
\end{aligned} \tag{A10}$$

Their corresponding static expressions are:

$$u^{CT}(q) = \int dr r^2 j_0(qr) [g^2(r) + f^2(r)], \tag{A11}$$

$$u^{CS}(q) = \int dr r^2 \frac{j_1(qr)}{q} g(r) f(r). \tag{A12}$$

Finally, the relationships between the electromagnetic form factors and the partial-wave decomposed radial potentials are:

$$v_L^{CT}(k', k) = \int_{-1}^1 dx P_L(x) u^{CT}(q), \tag{A13}$$

$$v_0^{CS}(k', k) = 0, \tag{A14}$$

$$v_1^{CS}(k', k) = \frac{k'k}{6} \int_{-1}^1 dx [1 - P_2(x)] u_{CS}(q). \tag{A15}$$

REFERENCES

- [1] N. Isgur and G. Karl, Phys. Rev. D **21**, 3175 (1980).
- [2] A. Chodos et al., Phys. Rev. D **9**, 3471 (1974); *ibid.* D **10**, 2599 (1974).
- [3] L. Wilets, *Non-Topological Solitons*, World Scientific, Singapore (1989); M. C. Birse, Prog. in Part. and Nucl. Phys.,**25**, 1 (1990).
- [4] A. W. Thomas, Adv. in Nucl. Physics, **13**, 1 (1984); G. A. Miller, Int. Rev. of Nucl. Phys., edited by W. Weise, **1**, (1984).
- [5] A. W. Thomas, S. Theberge and G. A. Miller, Phys. Rev. D **24**, 216 (1981).
- [6] E. A. Veit, B. K. Jennings and A. W. Thomas, Phys. Rev. D **33**, 1859 (1986).
- [7] G. He and R. H. Landau, Phys. Rev. C **48**, 3047 (1993).
- [8] H. B. Nielsen and A. Patkos, Nucl. Phys. **B195**, 137 (1982).
- [9] G. Krein, P. Tang, L. Wilets and A. G. Williams, Nucl. Phys., **A523**, 548 (1991).
- [10] S. Sahu and S. C. Phatak, Mod. Phys. Letts. A **7**, 709 (1992); S. Sahu, Ph. D. Thesis, Utkal University, Bhubaneswar.
- [11] A. G. Williams and L. R. Dodd, Phys. Rev. D **37**, 1971 (1988).
- [12] R. E. Peierls and J. Yoccoz, Proc. Phys. Soc. (London), **A70**, 381 (1957).
- [13] M. Bickeboller, M. C. Birse, H. Marschall, and L. Wilets, Phys. Rev. D **31** 2892 (1985); M. Bickeboller, R. Goldflam and L. Wilets, J. Math. Phys. **26**, 1810 (1985).
- [14] F. E. Close, *An Introduction to Quarks and Partons*, Academic Press, London (1979); M. Guidry, *Gauge Field Theories*, Wiley, New York (1991).
- [15] T. DeGrand, R. L. Jaffe, K. Johnson, and J. Kiskis, Phys. Rev. D **12**, 2060 (1975).
- [16] Particle Data Group, Rev. of Part. Properties, Phys. Rev. D **50**, 1670 (1994).

- [17] T.-S. H. Lee, private communication.
- [18] PN934f PI-N data VPI&SU 11/93 Arndt, physics@vtintc.phys.vt.edu.
- [19] J. A. Elsey and I. R. Afnan, Phys. Rev. D **40**, 2353 (1989).
- [20] B. C. Pearce and I. R. Afnan, Phys. Rev. C **40**, 220 (1989); *ibid.* C **34**, 991 (1986).
- [21] E. D. Cooper and B. K. Jennings, Phys. Rev. D **33**, 1509 (1986).
- [22] H. J. Pirner, Prog. in Part. and Nucl. Phys, **29**, 33 (1992).

TABLES

TABLE I. One-pion spin-flavor coupling constants.

λ_{BMB_0}	
	$\pi\Delta$
N	$4\sqrt{2}$
Δ	5

TABLE II. Two-pion spin-flavor coupling constants.

	$\lambda_{\beta\alpha}^{TI}$				$\lambda_{\beta\alpha}^{SI}$			
	$I = \frac{1}{2}$		$I = \frac{3}{2}$		$I = \frac{1}{2}$		$I = \frac{3}{2}$	
	πN	$\pi\Delta$	πN	$\pi\Delta$	πN	$\pi\Delta$	πN	$\pi\Delta$
πN	-1	0	$\frac{1}{2}$	0	$-\frac{5}{3}$	$-\frac{2\sqrt{2}}{3}$	$\frac{5}{6}$	$-\frac{2\sqrt{5}}{3}$
$\pi\Delta$	0	$-\frac{5}{2}$	0	-1	$-\frac{2\sqrt{2}}{3}$	$\frac{5\sqrt{10}}{6}$	$-\frac{2\sqrt{5}}{3}$	$\frac{\sqrt{10}}{3}$

TABLE III. Fitted parameters and deduced bare masses for the CDM.

f (MeV)	α_s	m_{gb} (MeV)	$m_N^{(0)}$ (MeV)	$m_\Delta^{(0)}$ (MeV)
90	0.112	1178	1239	1489
93	0.126	1127	1171	1439

TABLE IV. S and P wave scattering lengths in fm where $(ka_\alpha)^{2L+1} = \tan \delta_\alpha$.

$L_2 I_1 J$	a_{CDM} ($f=90$ MeV)	a_{CDM} ($f=93$ MeV)	a_{Born}	a_{CBM}	Exp.
S_{11}	+0.398	+0.342	0.237	+0.42	+0.243
S_{31}	-0.098	-0.093	-0.119	-0.07	-0.130
P_{11}	-0.892	-0.860	0.954		-0.569
P_{31}	-0.412	-0.420	-0.426		-0.483
P_{13}	-0.355	-0.366	-0.357		-0.375
P_{33}	+0.713	+0.712	0.583		+0.839

FIGURES

FIG. 1. The linear and quadratic term in $1/f$ contributing to the interaction Hamiltonian.

FIG. 2. The three lowest-order terms of the potential contributing to πN scattering.

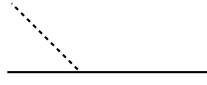
FIG. 3. (*Top*) The relation between the πNN coupling constant and the pion decay constant f . (*Bottom*) The πNN form factor for two different values of the pion decay constant f .

FIG. 4. The πNN form factors deduced from the behavior of the T matrix near the nucleon pole.

FIG. 5. The S- and P-wave πN phase shifts. The solid and dashed curves are for parameter sets with $f=90$ and $f=93$ respectively, and the dots are the experimental phase shifts.

This figure "fig1-1.png" is available in "png" format from:

<http://arxiv.org/ps/nucl-th/9412021v1>



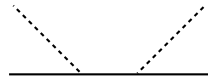
(a)



(b)

This figure "fig1-2.png" is available in "png" format from:

<http://arxiv.org/ps/nucl-th/9412021v1>



N, N^*, Δ

(a)



N, N^*, Δ

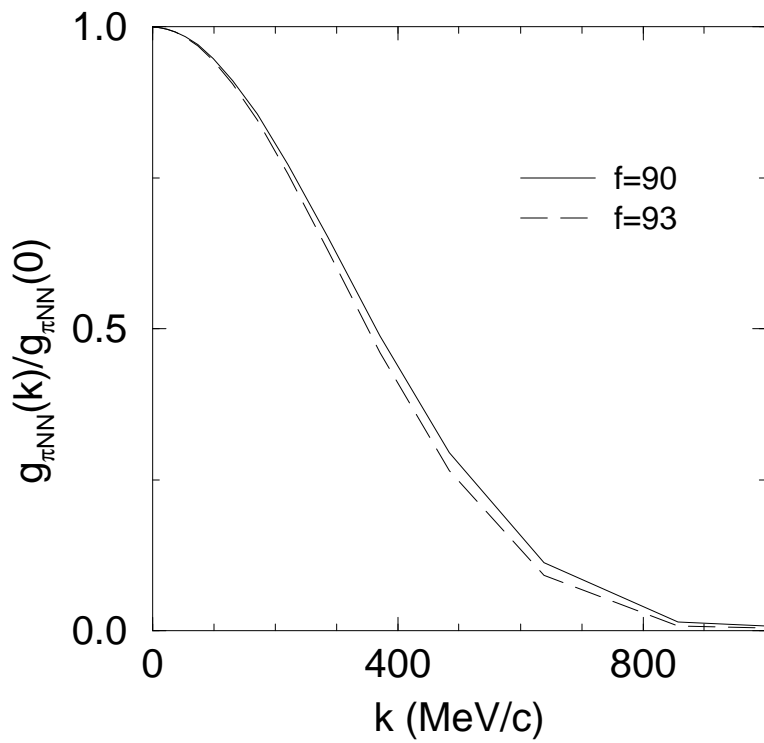
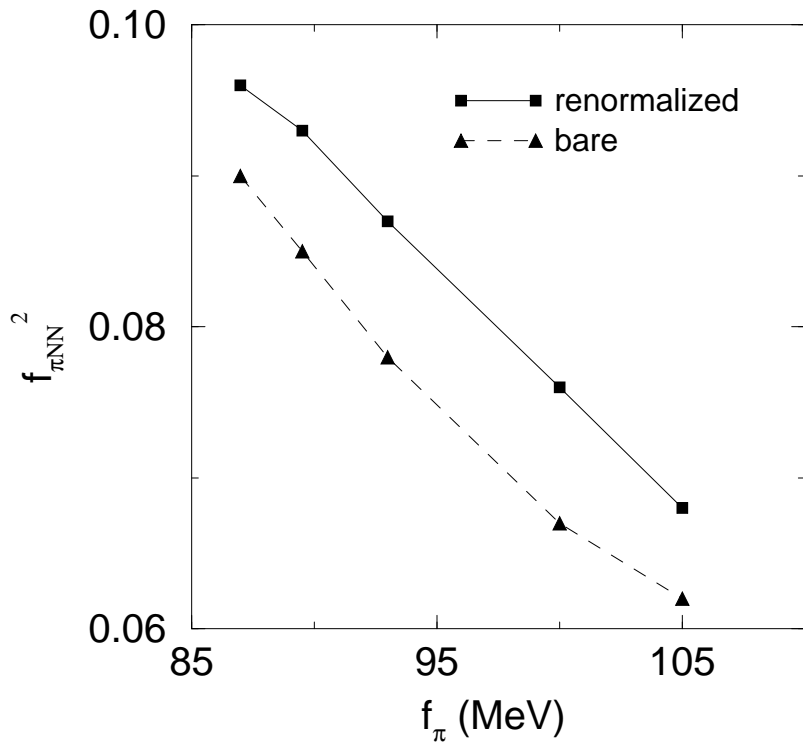
(b)



(c)

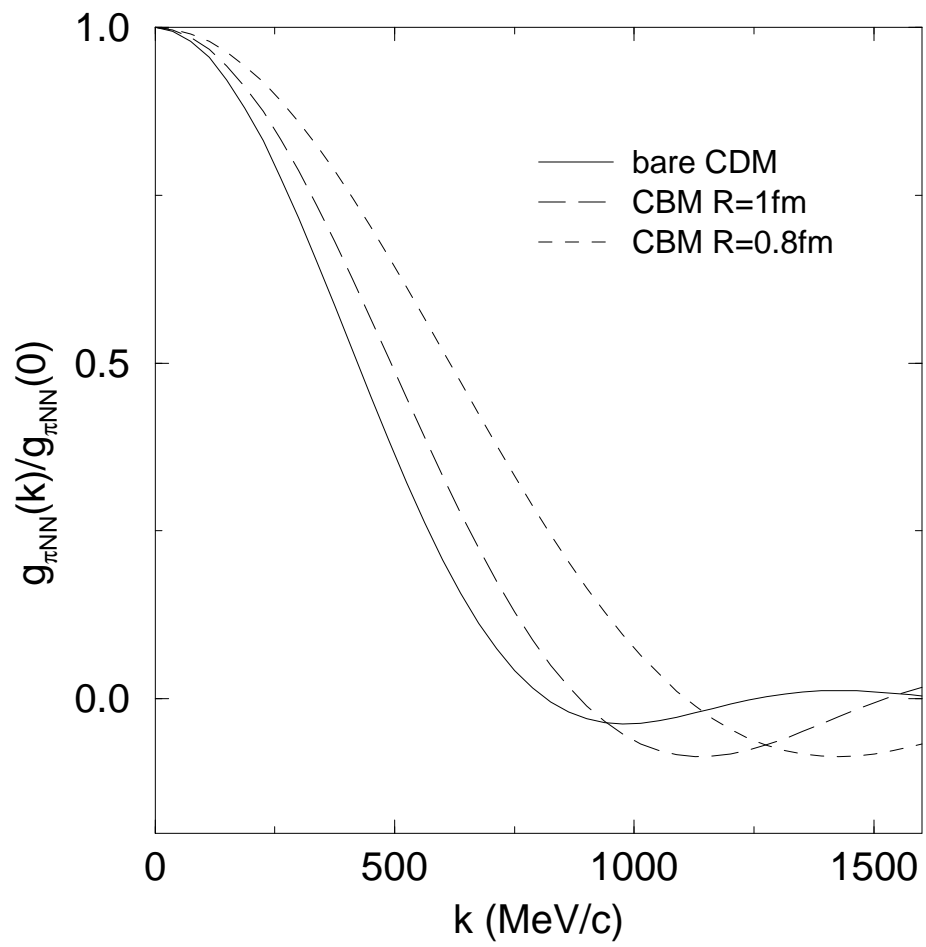
This figure "fig1-3.png" is available in "png" format from:

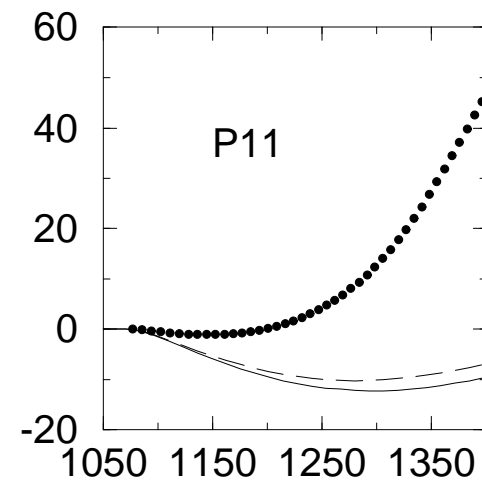
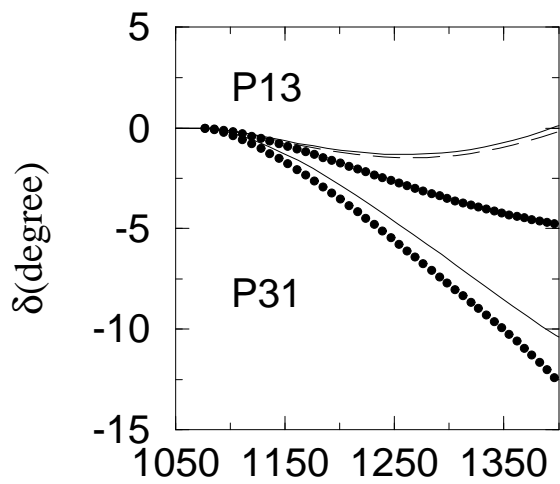
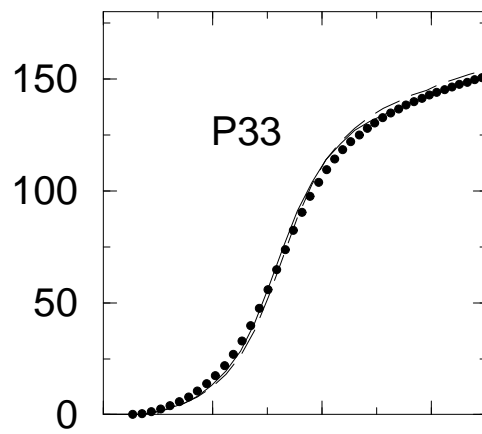
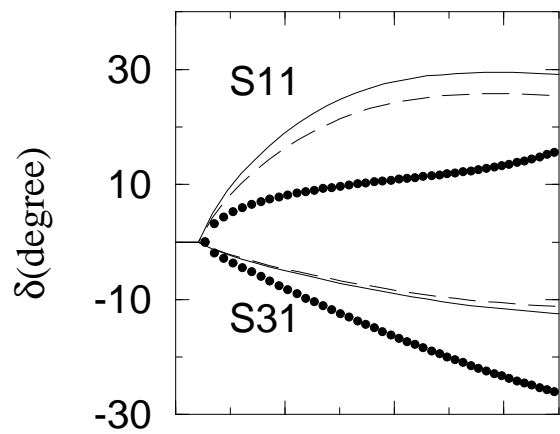
<http://arxiv.org/ps/nucl-th/9412021v1>



This figure "fig1-4.png" is available in "png" format from:

<http://arxiv.org/ps/nucl-th/9412021v1>





E_{CM} (MeV)